Broad Vitamin B6-Related Metabolic Disturbances in a Zebrafish Model of Hypophosphatasia (Alpl-Deficiency)

Jolita Ciapaite *, Monique Albersen, Sanne M. C. Savelberg, Marjolein Bosma, Nils W. F. Meijer, Federico Tessadori, Jeroen P. W. Bakkers, Gijs van Haaften, Judith J. Jans, Nanda M. Verhoeven-Duif

Posted Date: 7 March 2025

doi: 10.20944/preprints202503.0480.v1

Keywords: vitamin B6; hypophosphatasia; alpl deficiency; zebrafish; direct-infusion high-resolution mass spectrometry

 doi:10.20944/preprints202503.0480.v1

Article

Broad Vitamin B_6-Related Metabolic Disturbances in a Zebrafish Model of Hypophosphatasia (ALPL-Deficiency)

Jolita Ciapaite [1,*], Monique Albersen [1,†], Sanne M. C. Savelberg [1], Marjolein Bosma [1], Nils W. F. Meijer [1], Federico Tessadori [2], Jeroen P. W. Bakkers [2,3], Gijs van Haaften [1], Judith J. Jans [1] and Nanda M. Verhoeven-Duif [1]

[1] Department of Genetics, University Medical Center Utrecht, 3584 EA Utrecht, The Netherlands
[2] Hubrecht Institute-KNAW and University Medical Center Utrecht, 3584 CT Utrecht, The Netherlands
[3] Department of Medical Physiology, University Medical Center Utrecht, 3584 CM Utrecht, The Netherlands
* Correspondence: j.ciapaite@umcutrecht.nl
† Current address: Department of Laboratory Medicine, Amsterdam UMC location AMC, 1105 AZ Amsterdam, The Netherlands.

Abstract: Hypophosphatasia (HPP) is a rare inborn error of metabolism caused by pathogenic variants in *ALPL*, coding for tissue non-specific alkaline phosphatase. HPP patients suffer from impaired bone mineralization and in severe cases from vitamin B_6-responsive seizures. To study HPP we generated *alpl*$^{-/-}$ zebrafish line using CRISPR/Cas9 gene-editing technology. At 5 days post fertilization (dpf) no *alpl* mRNA and 89% lower total alkaline phosphatase activity was detected in *alpl*$^{-/-}$ compared to *alpl*$^{+/+}$ embryos. The survival of *alpl*$^{-/-}$ zebrafish was strongly decreased. Alizarin red staining showed decreased bone mineralization in *alpl*$^{-/-}$ embryos. B_6 vitamer analysis revealed depletion of pyridoxal and its degradation product 4-pyridoxic acid in *alpl*$^{-/-}$ embryos. Accumulation of d3-pyridoxal 5'-phosphate (d3-PLP) and reduced formation of d3-pyridoxal in *alpl*$^{-/-}$ embryos incubated with d3-PLP confirmed Alpl involvement in vitamin B_6 metabolism. Locomotion analysis showed pyridoxine treatment-responsive spontaneous seizures in *alpl*$^{-/-}$ embryos. Metabolic profiling of *alpl*$^{-/-}$ larvae using direct-infusion high-resolution mass spectrometry showed abnormalities in polyamine and neurotransmitter metabolism, suggesting dysfunction of vitamin B_6-dependent enzymes. Accumulation of N-methylethanolaminium phosphate indicated abnormalities in phosphoethanolamine metabolism. Taken together, we generated first zebrafish model of HPP that shows multiple features of human disease and is suitable to study pathophysiology of HPP and to test novel treatments.

Keywords: vitamin B_6; hypophosphatasia; alpl deficiency; zebrafish; direct-infusion high-resolution mass spectrometry

1. Introduction

Hypophosphatasia (HPP) is a rare inborn error of metabolism that affects the development of bones and teeth and is caused by pathogenic variants in *ALPL* gene, coding for the alkaline phosphatase, tissue-nonspecific isozyme (TNSALP, EC:3.1.3.1). Since the first description by Rathbun [1], more than 400 variants in *ALPL*, predominantly missense, have been identified [2], explaining highly variable clinical phenotype of HPP. Both autosomal recessive and autosomal dominant mode of inheritance has been reported, with the former often, but not always, corresponding to a more severe clinical phenotype [3]. TNSALP is expressed in liver, bone (synthesized by the osteoblasts), kidney, as well as brain [4] and it functions as a homodimeric ectoenzyme with a broad phospho-substrate specificity [5]. Natural substrates of TNSALP include, but likely are not limited to [5],

 doi:10.20944/preprints202503.0480.v1

inorganic pyrophosphate (PP_i) [6,7], pyridoxal 5'-phosphate (PLP, the active form of vitamin B_6) [8–10] and phosphoethanolamine [8,11,12]. The severity of clinical phenotype strongly correlates with the residual TNSALP enzyme activity [3,5,13]. Increased levels of plasma PLP and urinary and plasma PEA along with reduced serum unfractionated alkaline phosphatase activity serve as diagnostic markers of HPP [5,14].

Accumulation of TNSALP substrates in HPP patients reflects the physiological role of the enzyme and clarifies metabolic basis of HPP. Based on the age of diagnosis/onset of symptoms and severity of clinical phenotype HPP is classified in: perinatal (benign), perinatal (severe), infantile, childhood (mild), childhood (severe), adult and odontohypophosphatasia, with perinatal (severe) and infantile forms being most severe [14]. The main clinical feature of HPP is abnormal bone mineralization causing premature loss of deciduous teeth, rickets in children and osteomalacia in adults. The bone phenotype of HPP is explained by accumulation of PP_i, a potent inhibitor of bone mineralization [15]. Paradoxically, in some cases, premature closure of cranial sutures (craniosynostosis) occurs in infantile and childhood HPP causing intracranial hypertension [5,16]. In addition, blocked entry of minerals into the skeleton may lead to hypercalcemia/hypercalciuria, nephrocalcinosis, and renal impairment [5,17]. In the most severe forms of perinatal and infantile HPP vitamin B_6-dependent seizures may occur, indicating a lethal prognosis [18–22]. The seizures begin in the first hours after birth, are refractory to standard anticonvulsant drugs, but are responsive to pyridoxine (unphosphorylated form of vitamin B_6) [18–22]. B_6-dependent seizures are explained by the role of TNSALP in the cellular uptake of PLP (phosphorylated form of vitamin B_6) [23], with the decreased TNSALP activity presumably leading to vitamin B_6 deficiency in the central nervous system (CNS) (Figure 1a). The correlation between the response to pyridoxine and the severity of pediatric HPP reinforces TNSALP's role in vitamin B_6 metabolism [24]. Other, less well understood neurological symptoms of HPP may include depression, memory loss, ADHD, anxiety, headache and sleep disturbance [25].

HPP is an incurable disease. In addition to symptomatic treatment, enzyme replacement therapy with asfotase alfa, a mineral-targeted human recombinant TNSALP, is available for treatment of the bone phenotype of HPP [5,26]. Therefore, understanding TNSALP function in the kidney, liver, brain and other soft tissues as well as the mechanistic basis of milder neurological symptoms of HPP is becoming more relevant to improve quality of life of HPP patients.

Zebrafish (*Danio rerio*) is a promising model organism to study human disease [27], including HPP [28,29]. Zebrafish have 4 genes coding for alkaline phosphatases: two for intestinal alkaline phosphatases *alpi.1* and *alpi.2* (gene duplication), one for alkaline phosphatase 3 *alp3* (also expressed in intestine), and one for tissue-nonspecific alkaline phosphatase *alpl*, which also shows high degree of genetic conservation with human *ALPL* [28,29]. In the present study we generated the first *alpl*$^{-/-}$ zebrafish line using CRISPR/Cas9 gene-editing technology. Biochemical and behavioral characterization of *alpl*$^{-/-}$ zebrafish showed that they display multiple features of infantile HPP, including decreased bone mineralization, abnormal vitamin B_6 metabolism, abnormalities in neurotransmitter levels and pyridoxine-responsive seizures, as well as N-methylethanolaminium phosphate accumulation. Therefore, this new animal model could be used to gain insight in less understood aspects of HPP pathophysiology as well as for rapid screening of novel treatments.

Preprints.org (www.preprints.org) | NOT PEER-REVIEWED | Posted: 7 March 2025 doi:10.20944/preprints202503.0480.v1

2. Results

2.1. Generation of the Alpl Knockout Zebrafish

The *alpl* knockout zebrafish were generated using CRISPR/Cas9 gene editing. Sanger sequencing of F1 embryos derived from outcrossing F0 mosaic zebrafish revealed a 10 base pair out-of-frame deletion (c.623_632del, p.Gln180fs), predicted to result in a truncated protein (Figure 1b and c). Sequencing results also showed an intact reference sequence at the CRISPR target site in exon 6. The genotyping results of all untreated 5 dpf old embryos used in the present study (n=1752) showed the following genotype distribution: 27% *alpl*$^{+/+}$, 51% *alpl*$^{+/-}$ and 22% *alpl*$^{-/-}$. Upon visual inspection at 5 dpf, *alpl*$^{-/-}$ embryos were morphologically normal, indistinguishable from *alpl*$^{+/+}$ and *alpl*$^{+/-}$ embryos. Compared to the *alpl*$^{+/+}$ embryos, ~50% ($p<0.0001$) less *alpl* mRNA was detected in *alpl*$^{+/-}$ and virtually no *alpl* mRNA in *alpl*$^{-/-}$ zebrafish embryos at 5 dpf (Figure 1d). Total alkaline phosphatase enzyme activity measured in the whole embryo extracts was 37% ($p<0.0001$) and 87% ($p<0.0001$) lower in *alpl*$^{+/-}$ and *alpl*$^{-/-}$ zebrafish embryos, respectively, compared to WT (Figure 1e). The contribution of other alkaline phosphatase isoforms, such as intestinal alkaline phosphatase encoded by *alpi.1* and *alpi.2*, and possibly alkaline phosphatase 3, which is also expressed in intestine, could explain the residual enzyme activity measured in *alpl*$^{-/-}$ embryos, since intestinal isoforms are insensitive to (-)-tetramisole HCl [30]. In contrast to WT (*alpl*$^{+/+}$) zebrafish, no Alpl protein was detected at 62.5 kDa (the predicted molecular weight of alpl protein (NP_957301.2)) by western blot in *alpl*$^{-/-}$ embryos at 5 dpf (Figure 1f).

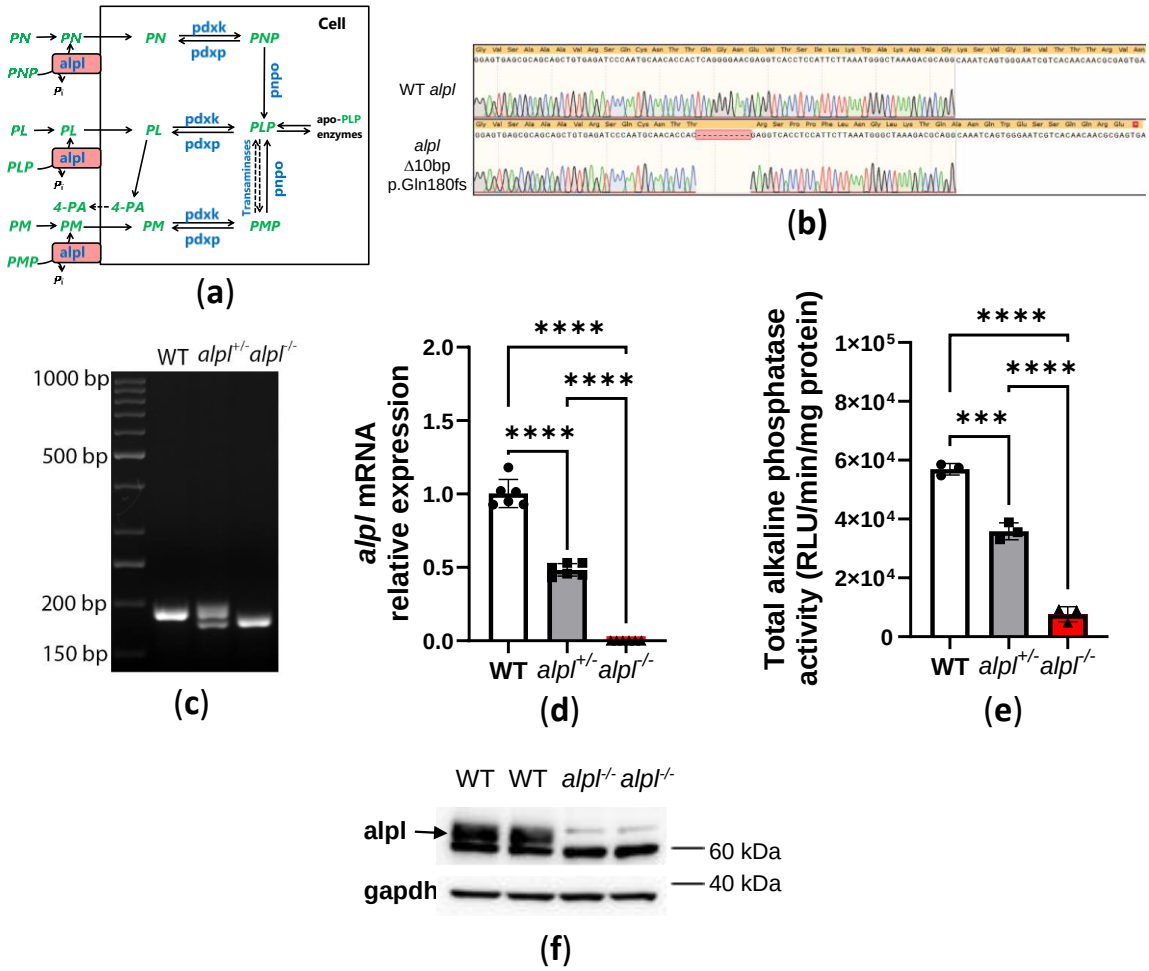

Figure 1. Generation and basic characterization of *alpl*$^{-/-}$ zebrafish line. (a) Schematic representation of vitamin B_6 metabolism. (b) Sanger sequencing results showing 10 bp deletion at the CRISPR site in exon 5 of *alpl* gene (c.623_632del, p.Gln180*fs*), which is predicted to result in a truncated protein. (c) Agarose electrophoresis of genotyping PCR products for the CRISPR site in exon 5 of *alpl* gene in wild type (WT), *alp*$^{+/-}$, *alpl*$^{-/-}$ 5 dpf old

 doi:10.20944/preprints202503.0480.v1

zebrafish embryos. (d) Relative *alpl* mRNA expression in WT, *alpl*$^{+/-}$ and *alpl*$^{-/-}$ 5 dpf old zebrafish embryos. Data are means from n=3 pools (10 embryos per pool) per genotype measured in duplicate ± SD. ****p<0.0001. (e) Total alkaline phosphatase activity in whole-embryo extracts of WT, *alpl*$^{+/-}$ and *alpl*$^{-/-}$ 5 dpf old zebrafish. RLU, relative light unit. Data are means from n=3 pools (10 embryos per pool) per genotype ±SD. ****p<0.0001 and ***p<0.001, (f) Alpl protein expression in total WT and *alpl*$^{-/-}$ 5 dpf zebrafish embryo extracts showing lack of alpl protein in *alpl*$^{-/-}$ embryos (predicted molecular weight of alpl protein (NP_957301.2) is 62.5 kDa). Data are from pools of n=32 embryos per genotype. Gapdh protein expression was used as the loading control.

2.2. *Abnormal Bone Mineralization, Vitamin B₆ Metabolism and Locomotion in alpl*$^{-/-}$ *Embryos*

Decreased bone mineralization due to accumulation of pyrophosphate, one of the substrates of TNSALP, is a key feature of HPP (7, 8). To determine the consequences of *alpl* knockout on bone mineralization, we stained 5 dpf embryos with acid-free alizarin red (bone) and alcian blue (cartilage) double stain. Less alizarin red staining of mineralized structures, such as notochord [31], in *alpl*$^{-/-}$ compared to WT and alpl$^{+/-}$ embryos at 5 dpf suggested negative effect of alpl deficiency on bone mineralization (Figure 2a).

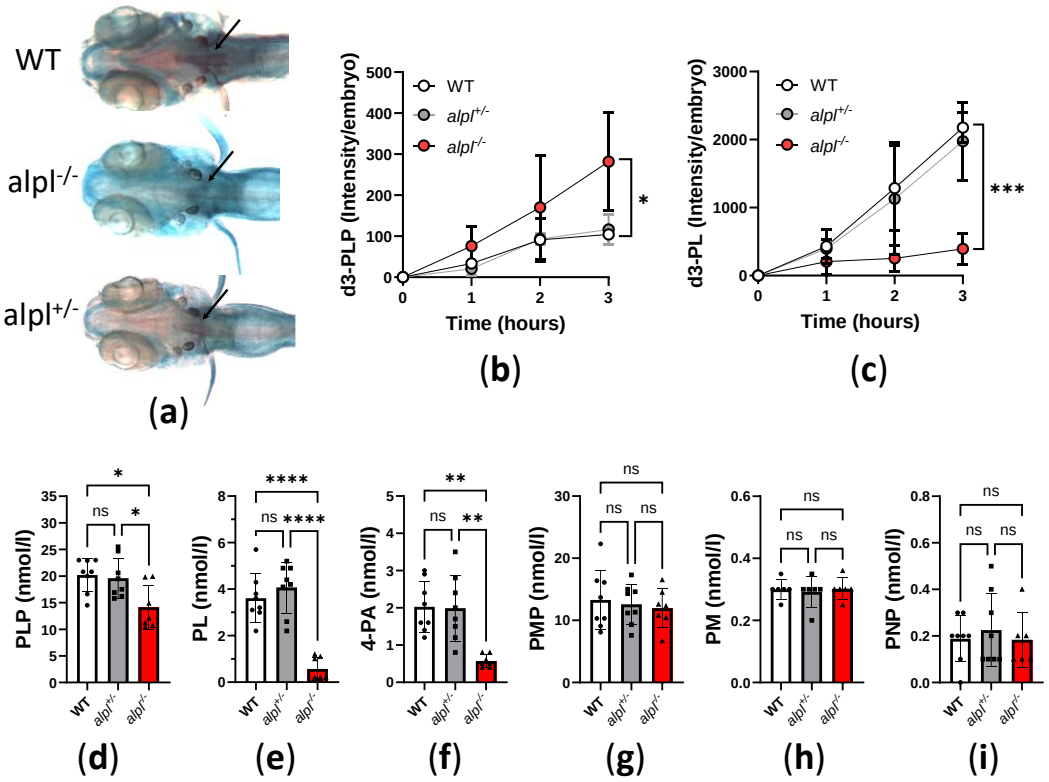

Figure 2. Impaired bone mineralization and abnormal vitamin B₆ metabolism in *alpl* knockout zebrafish. (a) Decreased alizarin red staining of mineralized structures (notochord, indicated by arrows) in *alpl*$^{-/-}$ compared to WT and *alpl*$^{+/-}$ embryos at 5 dpf suggests a negative effect of alpl deficiency on bone mineralization. (b) Accumulation of d3-PLP and (c) decreased production of d3-pyridoxal (d3-PL) in *alpl*$^{-/-}$ compared to WT and *alpl*$^{+/-}$ embryos incubated with 100 µM d3-PLP in embryo water (E3) for 3 hours at 28 °C. Data are means from n=3 pools (3 embryos per pool) per time point and genotype ± SD. (d) Steady-state PLP, (e) pyridoxal (PL), (f) 4-pyridoxic acid (4-PA), (g) pyridoxamine 5′-phospate (PMP), (h) pyridoxamine (PM) and (i) pyridoxine 5′-phosphate (PNP) concentrations in whole embryo extracts. Data are means from n=8 pools (3 embryos per pool) per genotype ± SD. ****p<0.0001, ***p<0.001 **p<0.01, *p<0.05 and ns—not significant (p>0.05).

Another important TNSALP substrate is extracellular (circulating) PLP (Figure 1a). We assessed the consequences of *alpl* knockout on PLP metabolism by measuring the utilization of d3-PLP by live

 doi:10.20944/preprints202503.0480.v1

5 dpf old embryos. After 3 hour incubation with 100 µM d3-PLP in embryo water, significantly more d3-PLP (Figure 2b) and significantly less d3-PL (Figure 2c) was observed in *alpl*$^{-/-}$ compared to WT and *alpl*$^{+/-}$ embryos, indicating impaired d3-PLP hydrolysis to d3-PL.

The steady-state PLP concentration measured in whole embryo extracts was slightly, but significantly lower in *alpl*$^{-/-}$ compared to WT and *alpl*$^{+/-}$ embryos (Figure 2d). Since Alpl deficiency is expected to result in increased PLP concentration in fluid extracellular matrix and decreased intracellular PLP concentration (see Figure 1a), the lower PLP concentration measured in whole *alpl*$^{-/-}$ embryo extracts likely indicates that cell-derived PLP dominated the total measured PLP. Concentrations of PL and its degradation product 4-PA were strongly decreased in *alpl*$^{-/-}$ compared to WT and *alpl*$^{+/-}$ embryos (Figure 2e and f, respectively), in agreement with the predicted negative effect of Alpl deficiency on both extra- and intracellular concentrations of these compounds. PMP concentration was not significantly changed in *alpl*$^{-/-}$ compared to WT and *alpl*$^{+/-}$ embryos (Figure 2g). Negligible concentrations of PM and PNP were measured in whole embryo extracts, which were similar in all tree genotypes (Figure 2h and i, respectively).

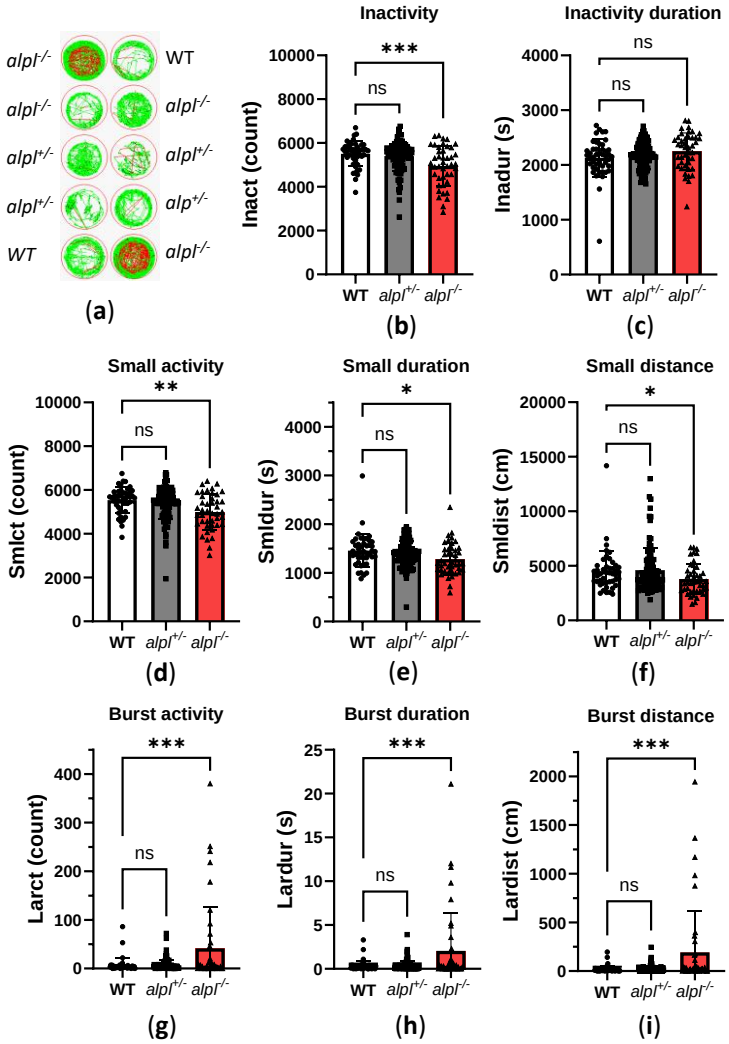

Figure 3 Locomotion analysis of 5 dpf old WT, *alpl*$^{+/-}$, *alpl*$^{-/-}$ zebrafish embryos. (a) Examples of swimming trajectories of 5 dpf old embryos recorded with Zebrabox for 1 hour at 28 °C in the dark. Green—movement speed <30 mm/s (small activity), red—movement speed >30 mm/s (burst activity), black—no movement (inactivity). (b) Inactivity count, (c) Duration of inactivity, (d) Small activity count, (e) Duration of small activity, (f) Distance swum during small activity, (g) Burst activity count, (h) Duration of burst activity, (i) Distance swum during burst activity. Data are means from n=45 (WT), n=105 (*alpl*$^{+/-}$) and n=42 (*alpl*$^{-/-}$) embryos ±SD. ***p<0.001, **p<0.01, *p<0.05 and ns—not significant (p>0.05).

 doi:10.20944/preprints202503.0480.v1

Intracellular PLP deficiency can have negative effects on neurotransmitter biosynthesis leading to vitamin B_6-dependent seizures [28]. In zebrafish embryos seizures cause typical fast, circular swimming bursts [32–35]. Therefore, we recorded the locomotion of 5 dpf old WT, *alpl*$^{+/-}$, *alpl*$^{-/-}$ embryos with a Zebrabox (Figure 3a and Supplemental Figure S1). Locomotion analysis revealed that inactivity count (i.e., number of times spent below the inactivity threshold) was significantly lower in *alpl*$^{-/-}$ compared to WT embryos (Figure 3b) without a change in the duration of inactivity (Figure 3c). Furthermore, the count, duration and distance swum in small movements (speed <30 mm/s) was significantly lower in *alpl*$^{-/-}$ compared to WT embryos (Figure 3d and e, respectively). In contrast, the count, duration and distance swum in burst movements (speed >30 mm/s) was significantly increased in *alpl*$^{-/-}$ compared to WT embryos (Figure 3g, h and i, respectively), indicating spontaneous seizures in the former. No locomotion parameters of *alpl*$^{+/-}$ embryos were significantly different from WT (Figure 3).

[32–35

Figure 4. Normalization of biochemical and locomotion abnormalities in 5 dpf old *alpl*$^{-/-}$ zebrafish embryos after 72 hours continuous treatment with 100 μM pyridoxine (PN). Concentrations of (a) pyridoxine (PN) (b) PLP, (c) pyridoxal (PL) and (d) 4-pyridoxic acid (4-PA) measured in whole 5 dpf old embryo extracts. Data are means from n=4-10 pools (3 embryos per pool) per genotype ± SD. Zebrabox analysis of (e) burst activity count, (f) duration of burst activity, (g) distance swum during burst activity in 5dpf old embryos measured for 1 hour at 28°C in the dark. Data are means from n=23-25 embryos per genotype and treatment ± SD. (h) γ-Aminobutyric acid (GABA) concentrations. Data are means from n=7-15 pools (3 embryos per pool) per genotype and treatment ± SD. (i) Fold-change analysis of amino acid concentrations in untreated *alpl*$^{-/-}$ and 100 μM PN-treated *alpl*$^{-/-}$ zebrafish embryos compared to the corresponding WT group. Data are from n=4 pools (3 embryos per pool). ****p<0.0001, ***p<0.001, **p<0.01, *p<0.05 and ns—not significant (p>0.05).

2.3. Pyridoxine Treatment Normalizes Locomotion and Some Metabolic Abnormalities in alpl$^{-/-}$ *Zebrafish Embryos*

Next, we investigated how vitamin B_6 treatment affects locomotion and biochemical abnormalities in 5 dpf old *alpl*$^{-/-}$ zebrafish embryos. Initial experiments showed no significant effects of a single, 3-hour treatment with 100 μM pyridoxine (PN) on B_6 vitamers and locomotion parameters in WT and *alpl*$^{-/-}$ embryos (data not shown). Increasing the duration of the treatment with 100 μM PN to 72 hours resulted in a strong increase in PN concentrations of a similar magnitude in WT and *alpl*$^{-/-}$ embryos (Figure 4a). PN-treatment had no significant effect on the PLP concentration in WT embryos (Figure 4b). In contrast, in *alpl*$^{-/-}$ embryos PN treatment led to an increase in PLP concentration to a level that was significantly higher than in WT (Figure 4b). Concentrations of PL and its degradation product 4-PA increased in both WT and *alpl*$^{-/-}$ embryos in response to PN treatment (Figure 4c and d, respectively). However, accumulation of both PL and 4-PA was less pronounced in *alpl*$^{-/-}$ embryos (Figure 4c and d, respectively). Concentrations of PM, PMP and PNP were not significantly affected by PN-treatment (Supplemental Figure S2a-c, respectively). Locomotion analysis showed that 72 hours of PN treatment resulted in significant reduction of parameters indicating spontaneous seizures in *alpl*$^{-/-}$ embryos. Specifically, burst activity count (Figure 4e), duration of burst activity (Figure 4f) and distance swum during burst activity (Figure 4g) were significantly lower in PN-treated compared to untreated *alpl*$^{-/-}$ embryos, and were not significantly different from WT. Furthermore, the concentration of the inhibitory neurotransmitter γ-aminobutyric acid (GABA), which was significantly lower in untreated *alpl*$^{-/-}$ embryos, was restored after PN treatment to the WT level (Figure 4h). Since PLP is a cofactor in many enzymes involved in amino acid metabolism, we analyzed amino acids. Glutamate, glutamine and asparagine concentrations were significantly lower in untreated *alpl*$^{-/-}$ compared to WT embryos. These amino acids were normalized after 72 hours of PN treatment (Figure 4i and Supplemental Figure S3a). Methionine, the only amino acid that significantly accumulated in untreated *alpl*$^{-/-}$ embryos, was normalized to WT level after PN treatment (Figure 4i and Figure S3a). Furthermore, concentrations

 doi:10.20944/preprints202503.0480.v1

of several amino acids significantly increased, independent of the genotype, in response to PN-treatment (proline, alanine, valine, leucine, serine, tryptophan and histidine) and the concentration of only ornithine decreased, independent of the genotype, in response to PN-treatment (Figure S3b). The concentrations of the remaining quantified amino acids were not affected neither by genotype nor PN treatment (Supplemental Figure S3c).

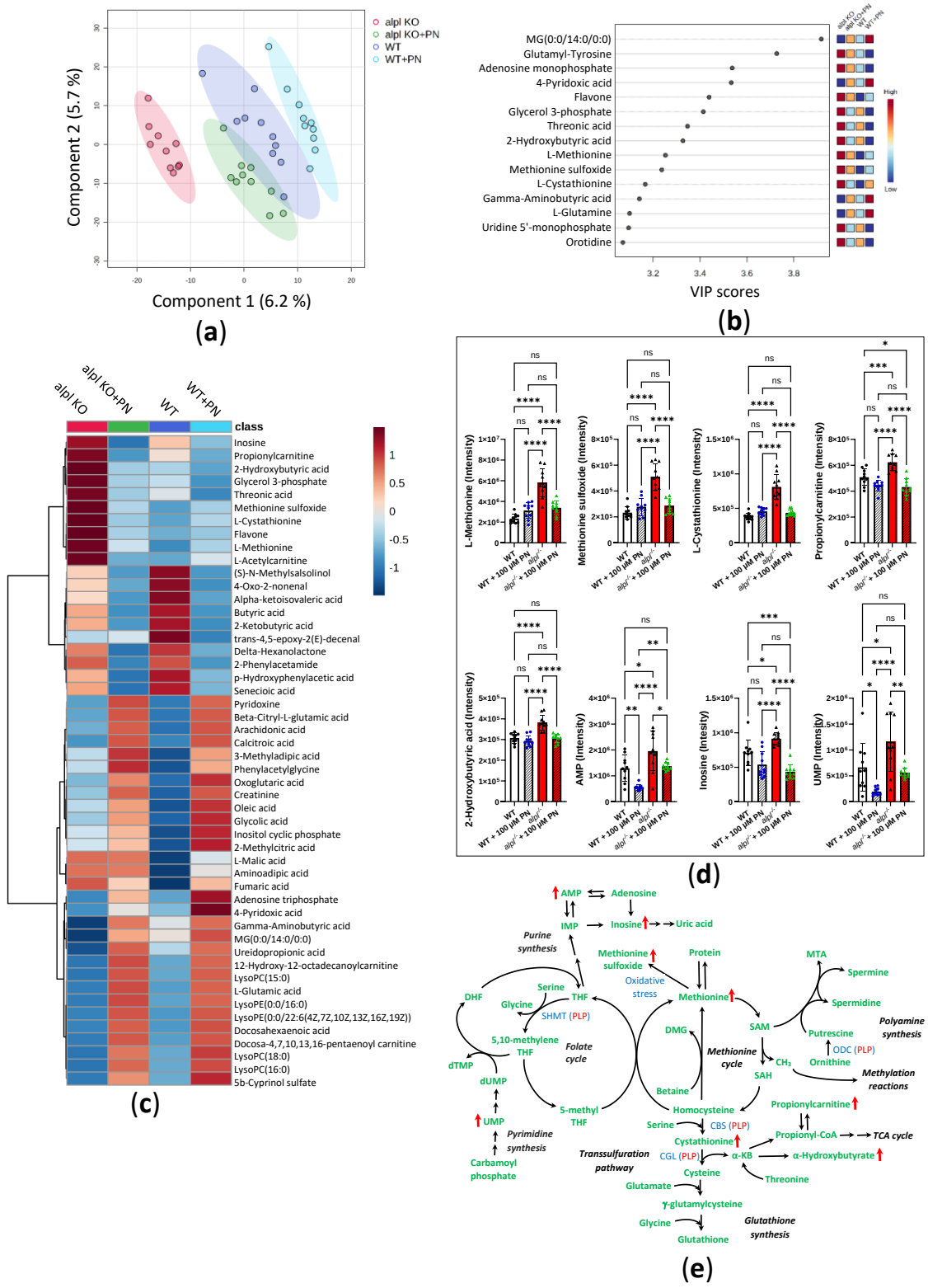

Figure 5. Global metabolic response to pyridoxine (PN) treatment in 5 dpf old WT and *alpl*$^{-/-}$ zebrafish embryos. (a) Partial least squares-discriminant analysis (PLS-DA) scores plot (principal component 1 (x-axis) and

 doi:10.20944/preprints202503.0480.v1

component 2 (Y-axis)). The explained variances are shown in brackets. 95% confidence intervals are shown for each group. (b) Important metabolites identified by PLS-DA for principal component 1. Metabolites with the highest variable importance in projection (VIP) scores are shown. The colored boxes on the right indicate the relative intensity of the corresponding metabolite in each group. (c) Heatmap visualization of group-average intensities of the 50 highest-ranking metabolites based on one-way ANOVA results. Euclidean distance and Ward's clustering algorithm were used for the hierarchical clustering of metabolites. (d) Intensities of a selection of the highest-ranking metabolites based on one-way ANOVA results. Data are means from n=10 pools (3 embryos per pool) per genotype and treatment group ± SD. ****p<0.0001, ***p<0.001, **p<0.01, *p<0.05 and ns — not significant (p>0.05); comparisons as indicated in the graphs. (e) Schematic visualization of metabolic pathways where strongest effects of Alpl deficiency were observed followed by normalization after pyridoxine treatment. Metabolites are shown in green; red arrows indicate the effect of alpl deficiency. Key PLP-dependent enzymes are shown in blue: SHMT, serine hydroxymethyltransferase (EC 2.1.2.1); CBS, cystathionine-β-synthase (EC 4.2.1.22); CGL, cystathionine γ-lyase (EC 4.4.1.1); ODC, ornithine decarboxylase (EC 4.1.1.17).

To explore global metabolic response to PN treatment we analyzed the metabolomes of untreated and 100 µM PN-treated WT and *alpl*$^{-/-}$ embryo extracts by direct-infusion high-resolution mass spectrometry (DI-HRMS). Using an in-house developed peak calling pipeline [36], 1919 mass peaks were annotated with 3941 metabolites that could occur endogenously. Partial least squares-discriminant analysis (PLS-DA) showed a clear discrimination of *alpl*$^{-/-}$ and WT metabolomes, which became less pronounced upon PN treatment, suggesting normalization of *alpl*$^{-/-}$ zebrafish metabolome after 72 hour treatment with 100 µM PN (Figure 5a). Among the metabolites of component 1, identified by PLS-DA as contributing the most to the separation of the data, were several phosphorylated compounds (adenosine monophosphate (AMP), glycerol 3-phosphate, uridine 5'-monophosphate (UMP)), the vitamin B_6 degradation product 4-pyridoxic acid (4-PA), as well as several amino acids and their derivatives (glutamine, GABA, methionine, methionine sulfoxide and cystathionine) (Figure 5b). Statistical analysis of the data using one-way ANOVA with Tuckey's post-hoc test identified 284 significantly altered metabolites (Supplemental Table S2). The heatmap overview of 50 highest-ranking metabolites based on one-way ANOVA results is shown in Figure 5c. Closer inspection of Tuckey's post-hoc test results showed that 144 metabolites identified by one-way ANOVA were significantly changed in *alpl*$^{-/-}$ embryos compared to WT, of which 64 metabolites were subsequently significantly affected by PN-treatment (Supplemental Table S2, Supplemental Figure S4a). Among phospho compounds that were increased in *alpl*$^{-/-}$ embryos compared to WT but did not respond to PN treatment and therefore could be directly related to the alpl phosphatase function were: inositol cyclic phosphate, cytidine monophosphate, phosphoguanidinoacetate, (S)-5-diphosphomevalonic acid, phosphodimethylethanolamine and glycerylphosphorylethanolamine (Supplemental Table S2). In contrast, the level of O-phosphoethanolamine normalized by PN treatment, indicating that its accumulation was caused by a different, vitamin B_6-dependent, mechanism (Supplemental Table S2). Figure 5d shows a selection of highest-ranking metabolites that were responsive to PN-treatment. The localization of these metabolites within the metabolic pathways is marked based on the KEGG pathway database information in Figure 5e. Abnormalities in methionine, its oxidation product methionine sulfoxide, and cystathionine levels in *alpl*$^{-/-}$ embryos (Figure 5d) suggested impaired functioning or methionine and/or folate cycles, and transsulfuration pathway, which in turn is important for synthesis of glutathione (Figure 5e). These pathways contain vitamin B_6-dependent enzymes, and the fact that all three metabolites were normalized after PN-treatment indicated that the effects were likely mediated by these enzymes. While glutathione levels were similar in WT and *alpl*$^{-/-}$ embryos, they significantly increased in both genotypes upon PN-treatment (Supplemental Figure S4b), indicating sensitivity of glutathione synthesis to vitamin B_6 availability. Increased levels of 2-hydroxybutyric acid and propionylcarnitine in *alpl*$^{-/-}$ embryos suggested that surplus cystathionine was diverted from the transsulfuration pathway, possibly due to impaired activity of vitamin B_6-dependent cystathionine-β-synthase (Figure 5d-e). Moreover, the impairment of transsulfuration pathway activity could

 doi:10.20944/preprints202503.0480.v1

underly elevation of N1-acetylspermidine level in *alpl*$^{-/-}$ embryos (Supplemental Figure S4c) by pushing the methionine cycle intermediates into the polyamine pathway (Figure 5e). While none of the measured canonic folate cycle intermediates were altered in *alpl*$^{-/-}$ embryos, we observed accumulation of 10-formyldihydrofolate (Supplemental Figure S4d), which was shown to participate in purine synthesis in mammalian cells [37]. Consequently, we found increased levels of AMP and inosine in *alpl*$^{-/-}$ embryos, which decreased after PN-treatment (Figure 5d-e). Additionally, PN-treatment responsive abnormalities in pyrimidine synthesis pathway intermediates UMP (Figure 5d-e) and orotidine (Supplemental Figure S4e) in *alpl*$^{-/-}$ embryos may have resulted from abnormal folate cycle activity (Figure 5e).

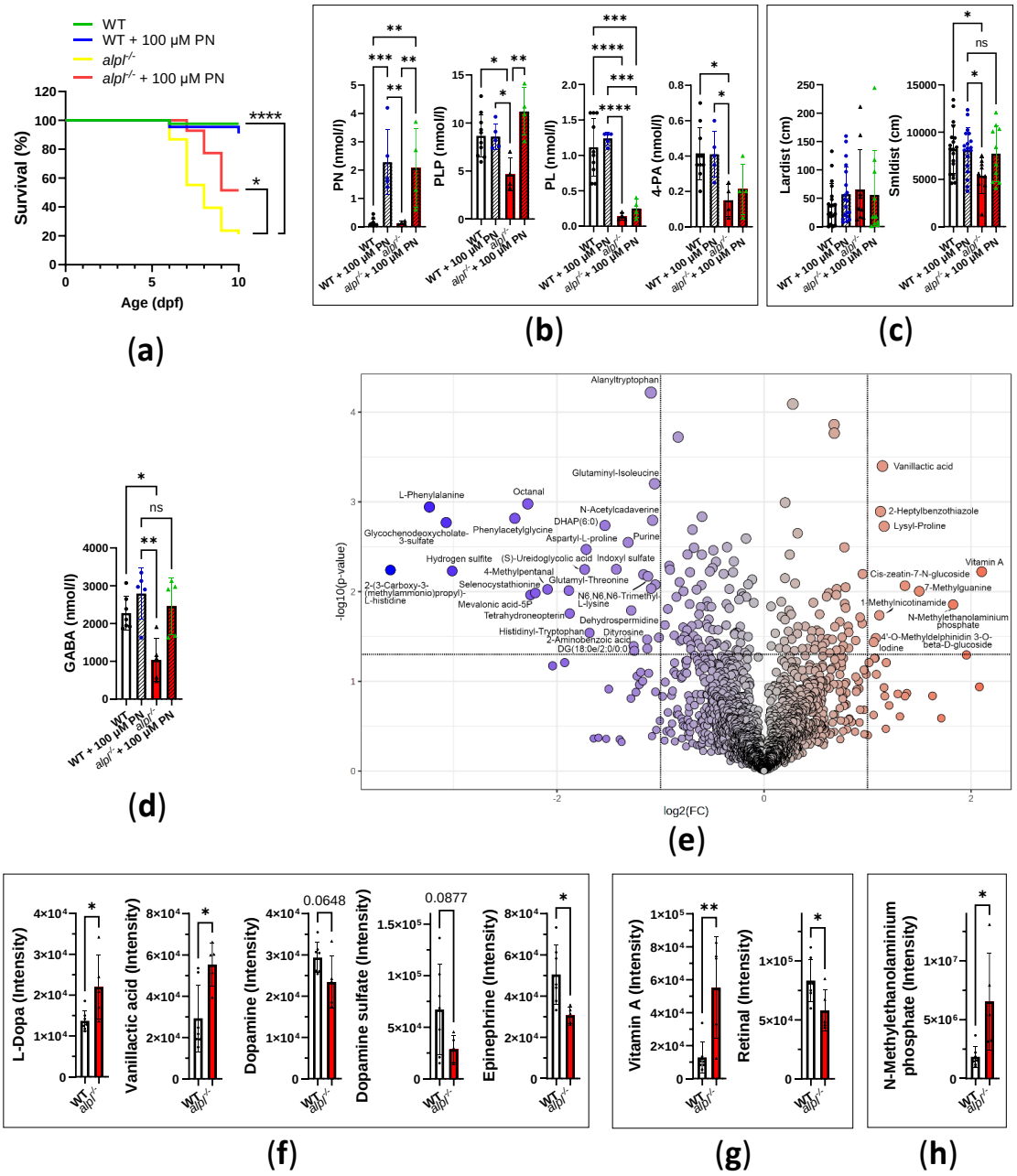

Figure 6. Progression of metabolic abnormalities in 10 dpf old *alpl*$^{-/-}$ zebrafish larvae. (a) Kaplan-Meier survival curves of untreated and 100 µM PN-treated WT and *alpl*$^{-/-}$ zebrafish until 10 dpf. Data are from n=18-42 zebrafish per genotype and treatment condition. (b) Concentrations of pyridoxine (PN), PLP, pyridoxal (PL) and its degradation product 4-pyridoxic acid (4-PA) in untreated and 100 µM PN-treated WT and *alpl*$^{-/-}$ larvae. Data are means from n=4-10 larvae per genotype and treatment condition ±SD. (c) Distance swum during burst activity

 doi:10.20944/preprints202503.0480.v1

(lardist, movement speed >30 mm/s) and during small activity (smldist, movement speed <30 mm/s) during 1 hour measurement using Zebrabox at 28°C in the dark. Data are means from n=9-19 larvae per genotype and treatment condition ±SD. (d) Concentrations of GABA in untreated and 100 µM PN-treated WT and *alpl*$^{-/-}$ larvae. Data are means from n=5-7 larvae per genotype and treatment condition ±SD. (e) Important features in metabolome of *alpl*$^{-/-}$ larvae selected by volcano plot with fold change (FC) threshold equal to 2 (x-axis) and t-tests threshold of $p<0.05$ (y-axis). (f) Accumulation of L-Dopa and vanillactic acid, and decreased level of dopamine, dopamine sulfate (dopamine 4-sulfate and dopamine 3-O-sulfate) and epinephrine in *alpl*$^{-/-}$ larvae suggest impaired activity of aromatic L-amino acid decarboxylase. (g) Accumulation of vitamin A (retinol) and decreased level of retinal in *alpl*$^{-/-}$ larvae. (h) Accumulation of N-methylethanolaminium phosphate in *alpl*$^{-/-}$ larvae. Data are means from n=5-7 larvae per genotype ±SD (panels E-H). ****$p<0.0001$, ***$p<0.001$, **$p<0.01$ and *$p<0.05$.

2.4. Progression of Metabolic Abnormalities and Decreased Survival in alpl$^{-/-}$ *Zebrafish Larvae*

To assess the progression of metabolic abnormalities we analyzed 10 dpf old WT and *alpl*$^{-/-}$ zebrafish larvae. Only 24% *alpl*$^{-/-}$ larvae were alive at 10 dpf (Figure 6a). Treatment with 100 µM PN for 5 days (from 5 dpf to 10 dpf, 30 min/day) led to significant improvement of survival of *alpl*$^{-/-}$ zebrafish larvae (Figure 6a), however, it did not restore the survival to WT levels. While this treatment regimen resulted in increases in PN and PLP concentrations in *alpl*$^{-/-}$ zebrafish larvae, the concentrations of PL and its degradation product 4-PA remained low (Figure 6b). Locomotion analysis using Zebrabox did not indicate spontaneous seizures during 1 hour measurement in the surviving larvae, as indicated by similar burst activity parameters in WT and *alpl*$^{-/-}$ larvae (Figure 6c and Supplemental Figure S5a). However, there was a decrease in all small activity parameters, i.e., distance swum in small movements (Figure 6c) as well as the count and duration of small movements in *alpl*$^{-/-}$ larvae (Supplemental Figure S5b), indicating decreased mobility of the mutants, which was normalized by PN treatment. No differences were observed in the inactivity count and duration (Supplemental Figure S5c). The concentration of GABA was lower in untreated *alpl*$^{-/-}$ larvae, but it was normalized by PN treatment (Figure 6d).

Next, we analyzed the metabolomes of 10 dpf old WT and *alpl*$^{-/-}$ larvae with DI-HRMS. Consequently, 1899 mass peaks were annotated with 3891 metabolites that could occur endogenously [36]. Statistical analysis using a t-test identified 183 metabolites significantly ($p<0.05$) altered in *alpl*$^{-/-}$ compared to WT larvae (Supplemental Table S3). Further analysis using a volcano plot identified several metabolites that were strongly and significantly changed in *alpl*$^{-/-}$ larvae (Figure 6e, Supplemental Table S4). Statistical analysis revealed abnormalities in several neurotransmitters, including decreased levels of GABA (Supplemental Table S3) and increased levels of L-DOPA in *alpl*$^{-/-}$ larvae (Figure 6f, Supplemental Table S3). Accumulation of L-DOPA in conjunction with the elevation of vanillactic acid (Figure 6f) pointed towards abnormal activity of PLP-dependent aromatic L-amino acid decarboxylase (AADC, EC: 4.1.1.28) [38]. Consequently, the downstream products of AADC activity dopamine and epinephrine were negatively affected by alpl deficiency (Figure 6f). 2-(3-Carboxy-3-(methylammonio)propyl)-L-histidine, a post-translationally modified histidine, that serves as a substrate for diphthine synthase (EC:2.1.1.98), a methyltransferase involved in transfer of one-carbon groups, was strongly decreased in *alpl*$^{-/-}$ larvae (Figure 6e, Supplemental Table S3-4). Furthermore, changed levels of several polyamine species (N-acetylcadaverine, N-acetylputrescine, dehydrospermidine and N1-acetylspermidine (all decreased) and norspermidine (increased)) in *alpl*$^{-/-}$ zebrafish larvae (Figure 6e, Supplemental Table S3-4) indicated altered activity of polyamine synthesis pathway. An increase in vitamin A (retinol) and decrease in retinal (oxidized form of retinol, component of visual pigment [39]) (Figure 6g, Supplemental Table S3-4) pointed towards abnormalities in vitamin A metabolism in *alpl*$^{-/-}$ larvae. Moreover, accumulation of N-methylethanolaminium phosphate in *alpl*$^{-/-}$ larvae (Figure 6h) suggested abnormal metabolism of phosphoethanolamines.

 doi:10.20944/preprints202503.0480.v1

3. Discussion

While the mechanistic basis of the bone phenotype of HPP is well understood, several unexplained clinical features remain, including craniosynostosis and neurological manifestations [22,25]. Moreover, the understanding of TNSALP function in the soft tissues like kidney, liver and brain is very limited, underscoring the need for further fundamental research. In the present study we described the first genetic model of tissue non-specific alkaline phosphatase deficiency in zebrafish that displayed many key features of human HPP. Our data showed that like TNSALP in humans, Alpl in zebrafish has a function in vitamin B_6 metabolism, as illustrated by strongly impaired ability of *alpl*$^{-/-}$ embryos to hydrolyze d3-PLP to d3-PL. The deficiency in Alpl activity led to lower total PLP, PL and 4-PA levels, and to vitamin B_6 (pyridoxine)-responsive seizures. Moreover, multiple metabolic abnormalities were identified through untargeted metabolomics that were linked to decreased cellular/tissue PLP levels and impaired activity of PLP-dependent enzymes. However, pyridoxine treatment improved, but not fully restored to WT level the survival of *alpl*$^{-/-}$ zebrafish. This suggests that deficiency of functions other than in vitamin B_6 metabolism (e.g., bone mineralization) played essential role in the lethality of alpl deficiency in zebrafish.

There is a high degree of evolutionary conservation of the gene coding for TNSALP in vertebrates [40,41], indicating that animal models of TNSALP deficiency can yield valuable insight in physiological functions of TNSALP and pathophysiology of HPP [29]. The murine models of TNSALP deficiency have already proven essential for the development of enzyme replacement therapy [42], which is currently the only available treatment option effective for bone phenotype of human HPP [26]. Zebrafish is increasingly used as an alternative model organism to study human diseases due to its ease of breeding, large number of offspring, and short generation time. The conservation of zebrafish Alpl function in skeleton and nervous system was previously postulated based on the comparison of tissue-specific gene expression patterns in zebrafish, mouse and human [41]. In the present study we describe the first genetic model of TNSALP deficiency in zebrafish generated using CRISPR/Cas gene editing. Although there was virtually no mRNA and protein detectable, there was residual alkaline phosphatase activity in 5dpf *alpl*$^{-/-}$ embryos. Since enzyme activity measurements were done in the total embryo extracts, the most plausible explanation of the residual activity is contribution of intestinal alkaline phosphatase (encoded by *alpi.1* and *alpi.2*) and alkaline phosphatase 3, also expressed in intestine, to the total measured enzyme activity. Residual alkaline phosphatase activity was also measured in serum of the first genetic murine model of TNSALP deficiency (*Akp2*$^{-/-}$), which was explained by the contribution of genetically distinct intestinal alkaline phosphatase activity [43]. Furthermore, the biochemical and behavioral characteristics of *alpl*$^{-/-}$ zebrafish described in the present study were comparable to the phenotypic features of *Akp2*$^{-/-}$ mice, which recapitulate lethal infantile HPP extremely well, including bone abnormalities and vitamin B_6-responsive seizures with untreated seizing animals dying before weening [43–45]. Data from available murine models of TNSALP deficiency show that in contrast to human TNSALP, murine TNSALP appears to be not essential for the initial events of bone mineralization during the intrauterine development (i.e., no severe skeletal abnormalities typical to perinatal HPP), but it becomes important for this process after birth [43–45]. In the present study we showed that zebrafish Alpl functions in bone mineralization, as indicated by decreased alizarin staining of notochord, one of the earliest mineralizing structures in zebrafish embryo [31]. This effect was comparable to the effect of chemical Alpl inhibition on bone mineralization in wild-type zebrafish embryos [41].

Vitamin B_6 (pyridoxine)-responsive seizures is a rare clinical feature of HPP, observed only in the most severe forms of perinatal and infantile HPP [18–22]. They are presumably caused by decreased PLP and PL availability in cells of central nervous system due to decreased/absent hydrolysis of extracellular PLP to PL (Figure 1a). Impaired activity of PLP-dependent enzymes involved in amino acid and neurotransmitter synthesis, e.g., decreased synthesis of the inhibitory neurotransmitter GABA due to lower activity of PLP-dependent glutamate decarboxylase (EC: 4.1.1.15), and resulting imbalance in the levels of inhibitory and excitatory neurotransmitters,

 doi:10.20944/preprints202503.0480.v1

underlies seizures [18,46,47]. Indeed, by using stably labeled PLP, we could show that the hydrolysis of PLP and production of PL is strongly impaired in *alpl*$^{-/-}$ embryos, leading to lower concentrations of PLP and PL, as well as 4-PA (degradation product of PL) in total embryo extracts (dominated by tissue derived PLP and PL). Unfortunately, due to the small size of the embryos we were unable to separately quantify PLP in the circulation and in the individual tissues. However, PLP deficiency in tissues including the brain were suggested by the observation that GABA concentrations in *alpl*$^{-/-}$ 5 dpf embryos and 10 dpf larvae were lower than in WT zebrafish, and they were normalized by PN treatment. The abnormalities in B_6 vitamer and GABA concentrations in *alpl*$^{-/-}$ zebrafish were in line with the findings in *Akp2*$^{-/-}$ mice, which have high serum PLP and low PL concentrations, as well as low PLP and PL concentrations in various tissues including the brain [43,44], and low brain GABA concentration [43]. In HPP patients circulating PLP concentration is elevated [9], making it a good biomarker of HPP [14], while PL concentration is less often reported, ranging from normal [18] to low in severe cases [10]. A single report in various post-mortem tissues of two patients with perinatal HPP showed no alterations in PLP and PL concentrations [10]. Lastly, similar to *Akp2*$^{-/-}$ mice [43–45] and severe forms of perinatal and infantile HPP [18–22], also *alpl*$^{-/-}$ zebrafish embryos developed spontaneous seizures that were responsive to PN treatment. However, we detected no spontaneous seizures in 10 dpf *alpl*$^{-/-}$ larvae, possibly which may be attributed to the fact that the measurements in larvae were done in a small number of the surviving larvae. Only subpopulation of *Akp2*$^{-/-}$ mice experience seizures [43]. The underlying cause of phenotypic heterogeneity despite of genetic homogeneity is not clear. We showed that, similarly to *Akp2*$^{-/-}$ mice [43–45] and HPP patients [18–22], spontaneous seizures in *alpl*$^{-/-}$ zebrafish embryos were responsive to PN treatment leading to improved survival of the mutants. The lack of complete rescue of the survival by PN treatment is in line with the multiple non-overlapping TNSALP functions, as demonstrated in *Akp2*$^{-/-}$ mice where PN treatment prevents seizures without beneficial effect on the skeletal phenotype [48].

The untargeted metabolomics analysis of broader consequences of Alpl deficiency showed abnormalities in several neurotransmitter levels attributable to decreased cellular PLP availability. Next to lower GABA levels, increased levels of L-DOPA and vanillactic acid along with lower levels of dopamine and epinephrine pointed towards decreased activity of PLP-dependent AADC in *alpl*$^{-/-}$ larvae. Impaired AADC activity was also implied in HPP patients based on elevated 3-ortho-methyldopa in CSF [18,47] and increased vanillactic acid in urine [47]. Moreover, we observed that accumulation of N-methylethanolaminium phosphate (PEA) is detectable in *alpl*$^{-/-}$ larvae but not yet in 5 dpf embryos, indicating that in zebrafish accumulation of PEA develops gradually.In *Akp2*$^{-/-}$ mice elevated serum PEA concentrations were shown in 8-10 day old pups, however, the age-dependence was not investigated [43]. Furthermore, we found increased methionine and cystathionine levels in *alpl*$^{-/-}$ embryos, suggesting altered activity of methionine cycle and transsulfuration pathway, likely caused by the impaired activity of PLP-dependent enzymes, as underscored by the normalization of these metabolites in response to PN-treatment (Figure 5E). Interestingly, the elevation of methionine and cystathionine levels was also reported in the brains of 1 week old *Akp2*$^{-/-}$ mice [49], suggesting common underlying mechanisms in zebrafish and mouse. Furthermore, elevated AMP and inosine levels in *alpl*$^{-/-}$ embryos suggest abnormalities in purine metabolism that could be linked to the deficiency of the Alpl ectophosphatase function and to the mechanisms of chronic pain via an effect on circulating adenosine levels [50]. Our observation that PN treatment led to normalization of AMP and inosine levels in *alpl*$^{-/-}$ embryos suggested that changes in these compounds were caused by reduced vitamin B_6 availability rather than by the ectophosphatase activity of Alpl. However, empirical pyridoxine therapy for chronic fatigue and pain in four adult-onset HPP patients did not provide symptomatic relief (22), suggesting that the underlying mechanisms are vitamin B_6-independent. It must be noted that due to the contribution of isobaric compounds to the levels of AMP, inosine and adenosine (not changed in *alpl*$^{-/-}$ embryos, data not shown) determined with DI-HRMS, further analysis using a targeted method is required.

Lastly, we observed accumulation of vitamin A (retinol) and decreased levels of retinal in *alpl*$^{-/-}$ larvae. Interestingly, high *alpl* expression and alpl enzyme activity were observed in the eyes

 doi:10.20944/preprints202503.0480.v1

(especially lens and retina) of zebrafish embryos [41], as well as retina of other vertebrates [51], suggesting that TNSALP has a function in vision. However, no eye-specific phenotype was reported in HPP patients or TNSALP deficient mice. Abnormalities in vitamin A metabolism have been implicated in development of craniosynostosis and skeletal abnormalities in humas and zebrafish [52]. The mechanistic basis of how Alpl deficiency leads to retinol accumulation needs further investigation. Possibly, impaired Ca^{2+} homeostasis caused by Alpl deficiency could affect retinol transport into the cell, which is regulated by Ca^{2+}/calmodulin [53], leading to accumulation of circulating retinol and decreased intracellular retinal production.

Taken together, we generated first zebrafish model of HPP that shows multiple features of human disease and is suitable to study pathophysiology of HPP and to test novel treatments. We showed that Alpl has a function in vitamin B_6 metabolism and bone mineralization in zebrafish. untargeted metabolomics revealed a multitude of metabolic alterations occurring in response to Alpl deficiency, including, but not limited to phosphoetanolamines, neurotransmitters, nucleotides, polyamines and retinoids suggesting potential interesting directions for follow-up research on the mechanisms of HPP in zebrafish. Furthermore, normalization of multiple metabolic abnormalities in response to PN treatment suggests that vitamin B_6 supplementation could be beneficial to HPP patients even in the absence of seizures. This study also revealed limitations of doing metabolic research in zebrafish embryos, particularly related to the small embryo size that constrained the ability to analyze individual tissues/organs. Nevertheless, data presented in this study clearly showed that this zebrafish model can serve as a valuable tool for investigating poorly understood aspects of TNSALP function and for developing improved therapies in the future.

4. Materials and Methods

4.1. Zebrafish Maintenance and Treatment Protocols

Zebrafish (*Danio rerio*) were raised and maintained under standard laboratory conditions [31]. Animal experiments were approved by and performed according to the guidelines of the Animal Welfare Body Utrecht, Utrecht University (protocol code 1444WP2B2).

Pyridoxine-treatment experiments were carried out in either 5dpf embryos and 10 dpf larvae. For embryo treatment, batches of 2 dpf embryos (not genotyped), generated by incrossing *alpl*$^{+/-}$ parents, were randomly assigned to untreated or pyridoxine-treated groups. Next, 0 μM (untreated) or 100 μM (treated) pyridoxine (Sigma-Aldrich) was added to E3 medium in a petri dish and embryos were raised to 5 dpf (3 days continuous treatment). Media were refreshed every 24 hours. At 5 dpf, embryos were anesthetized with tricaine, a sample of caudal fin was dissected for DNA isolation and genotyping, and embryos were instantly frozen on dry ice and stored at -80°C until analysis. For larvae treatment, zebrafish embryos were genotyped at 3 dpf as described in [34]. Only *alpl*$^{+/+}$ and *alpl*$^{-/-}$ embryos were raised to 5 dpf. Starting from 5 dpf, zebrafish were treated for 5 consecutive days (between 9.00 and 10.30 am) with 0 μM or 100 μM pyridoxine for 30 min. Treatment included placing zebrafish larvae (n=18-22 per tank) in plastic tanks containing 500 ml of system water without pyridoxine (untreated) or 500 ml of system water containing 100 μM pyridoxine (treated). After 30 min zebrafish larvae were rinsed and placed in the home tank. At 10 dpf zebrafish larvae were anesthetized with tricaine, terminated by instant freezing on dry ice (1 larva per Eppendorf cup) and stored at -80°C until analysis.

To assess the utilization of stably labeled pyridoxal 5′-phospate, 5 dpf old embryos (~60 embryos/petri dish) were incubated with 100 μM pyridoxal-5′-phosphate (methyl-D3) (d3-PLP) (Buchem, Minden, The Netherlands) in E3 for 0, 1, 2 and 3 hours. At specified time-points, embryos were washed with E3, anesthetized with tricaine, dissected for genotyping, snap-frozen on dry ice and stored at -80°C until analysis.

 doi:10.20944/preprints202503.0480.v1

4.2. sgRNA and Cas9 mRNA Design and Synthesis

CRISPR/Cas9 gene-specific regions for *alpl* were designed by the Sanger Institute (Hinxton, Cambridge, United Kingdom) using a modified version of CHOPCHOP (http://chopchop.cbu.uib.no). Target sites were selected in exon 5 and exon 6 (Supplemental Table S1) [54,55]. The gene-specific oligonucleotides contained the T7 promotor sequence (5'-TAATACGACTCACTATA-3'), the GGN20 target site without the Protospacer Adjacent Motif (PAM), and the constant complementary region 5'-GTTTTAGAGCTAGAAATAGCAAG-3'. Oligonucleotides were ordered at IDT (Integrated DNA Technologies, Coralville, Iowa, USA) and the zebrafish specific pCS2-nCas9n plasmid was obtained from Addgene (Cambridge, USA). Cas9 mRNA transcription and sgRNA synthesis were performed as described before [56].

4.3. Generation of Alpl Knockout Zebrafish

Wild type Tupfel longfin (WT TL) one-cell stage zebrafish embryos were microinjected in the yolk with approximately 1 nl sgRNA mixture (sgRNA targeting exon 5 and 6, each 30 ng/µl) and Cas9 mRNA (250 ng/µl). CRISPR efficiency was determined in subpopulation of healthy microinjected larvae at 4 dpf. The rest of the healthy microinjected larvae were raised till adulthood. Heterozygous variation was assessed in DNA extracted from healthy embryonal offspring (F1) at 24 dpf. Offspring from a mosaic founder that contained an 10 bp out-of-frame deletion was raised till adulthood and was fin-clipped for genotyping at 9 weeks of age. The mutant zebrafish line was maintained in the heterozygous form by crossing *alpl*$^{+/-}$ zebrafish with WT TL. In this study, F6 zebrafish (*alpl*$^{+/+}$, *alpl*$^{+/-}$ and *alpl*$^{-/-}$) were used, obtained from incrossing F5 *alpl*$^{+/-}$ zebrafish.

4.4. DNA Extraction and Genotyping

Depending on the type of experiment, genotyping was done on the caudal fin dissections at 3 or 5 dpf (overall experiments), whole 5 dpf embryos (Zebrabox and staining experiments), or adult zebrafish caudal fin dissections (line maintenance) as described in detail in [34]. Briefly, tissue was lysed in single embryo lysis buffer (SEL) containing 10 mM Tris pH 8.2, 10 mM EDTA. 200 mM NaCl, 0.5% sodium dodecyl sulfate (SDS) and 12 U/ml proteinase K (freshly added, Thermo Scientific, cat. # EO0491). DNA was isolated using the following thermocycler program: 60 min 60 °C, 15 min 95 °C, 15 min 4 °C, ∞ 12 °C. Genomic regions flanking the CRISPR target sites were amplified with CRISPR site-specific PCR primers (Table S1), using AmpliTaq Gold 360 DNA polymerase (Applied Biosystems, cat. # 4398823) in combination with a touch down PCR program as previously described [57]. Amplicons were visualized on a 3% agarose gel and mutations were confirmed by Sanger sequencing.

4.5. RNA Isolation and Real-Time PCR

Zebrafish embryos (5 dpf) were placed in sterile Eppendorf tubes on ice (10 embryos/tube per genotype, 3 tubes/genotype). Sterile, RNAse-free zirconium oxide beads (0.5 mm) and cold 0.5 ml TRI reagent (Sigma-Aldrich, cat. # T9424) were added to each tube. Embryos were homogenized using bullet blender tissue homogenizer (Next Advance) for 10 min in stand 8 at 4 °C. Total mRNA was isolated from the embryo homogenates following manufacturers recommendations. Quantity and purity of the total RNA was quantified using NanoDrop spectrophotometer (Thermo Scientific). 1 µg of total RNA was reverse transcribed to cDNA using M-MLV reverse transcriptase (Sigma-Aldrich, cat. # M1302) according to the manufacturer's protocol. Real-time PCR was done with StepOne Real-Time PCR System (Applied Biosystems, Waltham, MA, USA) using SYBR Select Master Mix (Applied Biosystems, cat. # 4472908) and primers listed in Table S1. The *alpl* (ZDB-GENE-040420-1, RefSeq:NM_201007.2) mRNA levels were normalized to the mRNA level of β-actin (ZDB-GENE-000329-1, RefSeq:NM_131031.2) and expressed relative to the wild type (calculated according to the ΔΔCt method).

 doi:10.20944/preprints202503.0480.v1

4.6. Alizarin Red and Alcian Blue Staining

Mineralized bone and cartilage were stained in whole 5dpf embryos with acid-free alizarin red and alcian blue double stain as described in [58]. Briefly, 5 dpf embryos were anesthetized with tricaine and up to 20 embryos were collected per 1.5 ml Eppendorf tube. After removing the medium, 1 ml of 4% paraformaldehyde in phosphate buffered saline was added per tube and embryos were fixed for 2 h with agitation at 500 rpm in an Eppendorf thermomixer at room temperature (RT), followed by washing and dehydration with 1 ml 50% ethanol for 10 min at RT. Embryos were stained overnight with 0.0005% alizarin red and 0.4% alcian blue working solution with agitation at RT. Stained embryos were washed and bleached with 1.5% H_2O_2 containing 1% KOH for 20 min at RT. After removing the bleach solution, 1 ml 20% glycerol containing 0.25% KOH was added and embryos were incubated for 2 hours, followed by overnight incubation with 1 ml 50 % glycerol containing 0.25% KOH at RT. Next, medium was replaced with 50% glycerol containing 0.1% KOH and embryos were stored at 4 °C. Images were captured with a Leica DFC420C digital microscope camera (Leica Microsystems, Wetzlar, Germany) mounted on a Zeiss Axioplan brightfield microscope (Carl Zeiss AG). After the imaging, DNA was extracted from stained embryos and genotype was determined as described in section 2.4.

4.7. Alkaline Phosphatase Enzyme Activity

Total alkaline phosphatase enzyme activity was determined in the whole embryo homogenates using assay described in [59]. Briefly, 5 dpf embryos (n=30 per genotype) were homogenized in 200 µl of Dulbecco's Phosphate Buffered Saline (DPBS, Sigma-Aldrich, cat. # D8537) containing 0.1% Triton X100 using bullet blender tissue homogenizer (Next Advance) for 5 min in stand 8 at 4 °C. Homogenates were centrifuged at 600 g for 5 min at 4 °C and sonicated using ultrasonic disintegrator (Soniprep 150 Plus, MSE) for 30 sec in the pulse mode (1 s on 1s off, amplitude 10 µm) on ice. Assay mix contained 20 µl embryo extract (5× diluted in DPBS, final protein concentration in the assay 0.065 mg/ml), 80 µl DPBS and 100 µl of CSPD ready-to-use reagent (0.25 mM solution; Roche GmbH, Mannheim, Germany, cat. # CSPD-RO) without Alpl inhibitor (-)-tetramisole HCl (Sigma-Aldrich, cat. # L9756) or with 20 mM (-)-tetramisole HCl. Alpl activity was measured by following the chemiluminescence for 5 min at 37 °C using Clariostar microplate reader (BMG Labtech). Alpl activity was expressed as RLU/min/mg protein. Protein concentration in the embryo homogenates was determined using Pierce BCA protein assay kit according to the manufacturers protocol (Thermo Scientific, cat. # 23225).

4.8. Western Blotting

Zebrafish embryos (5 dpf, n=32 per genotype) were placed in Eppendorf tubes on ice, 150 µl RIPA lysis and extraction buffer (Thermo Scientific, cat. #89900) containing 2 mM NaF (Sigma-Aldrich) and protease inhibitor cocktail (1:200, Roche) were added, followed by zirconium oxide beads (0.5 mm). Embryos were homogenized using bullet blender tissue homogenizer (Next Advance) for 10 min in stand 8 at 4 °C. Tissue homogenates were solubilized with agitation for 2 hours at 4 °C, followed by centrifugation at 16200 g for 10 min at 4 °C. Supernatants were mixed with LDS sample buffer (NuPage, Invitrogen, cat. # NP0007) and dithiothreitol (final concentration 50 mM), and denatured at 98 °C for 5 min with agitation. Proteins were resolved on NuPAGE 4-12% Bis-Tris gels (Invitrogen) and transferred to polyvinylidene difluoride (PVDF) membranes (Immobilon-P) with semi-dry blotting system (Novex, Invitrogen) following manufacturer's recommendations. Membranes were blocked with tris-buffered saline (TBS) containing 0.1% Tween 20 (TBS-T) and 50 g/l bovine serum albumin (BSA, Sigma-Aldrich) for 1 hour at RT. Next, the membranes were incubated overnight at 4 °C with primary rabbit polyclonal anti-ALPL antibody (1:1000, Sigma-Aldrich, cat. # HPA008765) or mouse monoclonal anti-glyceraldehyde-3-phosphate dehydrogenase (GAPDH, 1:5000, Santa Cruz Biotechnology, cat. # sc-365062) in TBS-T containing 10 g/l BSA. After washing 3 × 10 min with TBS-T, membranes were incubated with a corresponding horse-radish

 doi:10.20944/preprints202503.0480.v1

peroxidase-conjugated secondary antibody in TBS-T containing 5 g/l BSA for 1 hour at RT. After the final wash of 3 × 10 min with TBS-T, the immunocomplexes were detected using SuperSignal™ West Atto Ultimate Sensitivity Substrate (Thermo Scientific, cat. # A38554) and images were captured with the ChemiDoc MP imaging system (Bio-Rad Laboratories, Hercules, CA, USA).

4.9. B_6 Vitamer Analysis

Frozen zebrafish 5 dpf embryos (3 embryos/100 µl TCA) or 10 dpf larvae (1 larva/100 µl TCA) were homogenized in ice-cold trichloroacetic acid (TCA; 50 g/l) with zirconium oxide beads (0.5 mm) using a bullet blender tissue homogenizer (Next Advance) at a speed of 8 for 10 min at 4 °C. Homogenates were centrifuged at 16200 g for 5 min at 4 °C. Next, 80 µl of the supernatant was mixed with 80 µl of a solution containing stable isotope-labeled internal standards, vortexed, incubated for 15 min in the dark and centrifuged at 16200 g for 5 min at 4 °C. B_6 vitamers were quantified using ultra-performance liquid chromatography tandem mass spectrometry (UPLC-MS/MS) as previously described [60], except for using 10 times lower concentrations of the calibration samples. For the analysis of pyridoxal 5'-phosphate-(methyl-d3) (d3-PLP) utilization and pyridoxal-(methyl-d3) (d3-PL) formation, zebrafish embryos were processed and analyzed using the same protocol, except that no stable isotope-labeled internal standards were added during UPLC-MS/MS measurement. During all steps, samples were protected from light as much as possible.

4.10. Non-Quantitative Direct-Infusion High-Resolution Mass Spectrometry (DI-HRMS)

Metabolite profiling was done in 5 dpf embryos and 10 dpf larvae using a non-quantitative DI-HRMS method described in [36]. For extraction of metabolites, 3 embryos or a single 10 dpf larvae were homogenized in 100 µl of ice-cold 100% methanol with zirconium oxide beads (0.5 mm) using a bullet blender tissue homogenizer (Next Advance Inc., Averill Park, NY, USA) at a speed of 8 for 10 min at 4 °C. Homogenates were centrifuged at 16200 g for 5 min at 4 °C. The supernatants (70 µl) were mixed with 60 µL of 0.3% formic acid (Emsure, Darmstadt, Germany) and 70 µL of internal standard working solution described in [36], and filtered using a methanol-preconditioned 96-well filter plate (Pall Corporation, Ann Arbor, MI, USA) loaded onto a vacuum manifold into an Armadillo high-performance 96-well PCR plate (Thermo Fisher Scientific). Samples were analyzed using a TriVersa NanoMate system (Advion, Ithaca, NY, USA) controlled by Chipsoft software (version 8.3.3, Advion). Data were acquired using Xcalibur software (version 3.0, Thermo Scientific, Waltham,MA, USA). Raw mass spectrometry data were analyzed using an in-house developed peak calling pipeline written in R programming language (source code available at https://github.com/UMCUGenetics/DIMS) that utilizes Human Metabolome DataBase (HMDB) for peak annotation with the accuracy of 5 ppm with respect to the theoretical m/z value, as described in detail in [36]. The web-based analysis tool MetaboAnalyst v.6.0 was used for statistical analysis (one factor) [61]. Metabolites with multiple possible annotations (isobaric compounds) were processed as single metabolite for statistical purposes.

4.11. Amino Acid and γ-Aminobutyric Acid (GABA) Analysis

Amino acid analysis was performed in 40 µl of zebrafish embryo (3 embryos/100 µl) extracts in 100% methanol (see section 2.10 for preparation details) using an UPLC-MS/MS method described in [62]. GABA was quantified in 10 µl of zebrafish embryo (3 embryos/100 µl) or larvae (1 larva/100 µl) extracts in 100% methanol using an UPLC-MS/MS method described in [34].

4.12. Locomotion Analysis

Zebrabox system (Viewpoint Live Sciences, Lyon, France) was used to track and quantify the locomotion of zebrafish embryos. 5 dpf old embryos or 10 dpf old larvae (1 embryo/well) were transferred to a 48-wells flat-bottom plate (Greiner Bio-one CELLSTAR) containing 0.5 ml embryo medium E3 medium. Zebrafish embryos/larvae were allowed to acclimatize in the measurement

 doi:10.20944/preprints202503.0480.v1

chamber in the dark for 15 minutes prior to the measurement. Locomotion was assessed in the tracking mode using the following settings: background 15, inactivity threshold <1mm/s, and burst activity threshold >30 mm/s. Temperature was maintained at 28 ± 1 °C. Locomotion was tracked in the dark without any intervention for 1 hour. Movement trajectories were recorded and locomotion parameters were quantified with Zebralab software (Viewpoint Live Sciences, Lyon, France).

4.13. Statistical Analysis

Data are presented as means ± SD. Number of zebrafish used for specific experiment is indicated in the figure legends. Statistical analysis was performed using GraphPad Prism v.10 (GraphPad Software, San Diego, CA, USA). For comparison of two groups, Student's t-test was used. For comparison of three or more groups, one-way ANOVA followed by Tuckey's post hoc test was used. The level of significance was set at $p<0.05$.

Supplementary Materials: The following supporting information can be downloaded at the website of this paper posted on Preprints.org, Figure S1 Overview of swimming trajectories of 5 dpf old WT, *alpl*$^{+/-}$, *alpl*$^{-/-}$ zebrafish embryos; Figure S2 The effects of 72 hours continuous treatment with 100 μM pyridoxine on B_6 vitamers in 5dpf old WT and *alpl*$^{-/-}$ embryos; Figure S3 The effects of 72 hours continuous treatment with 100 μM pyridoxine (PN) on amino acid concentrations in 5dpf old WT and alpl-/- embryos; Figure S4. Analysis of DI-HRMS data; Figure S5 Locomotion parameters in untreated and 100 μM pyridoxine (PN)-treated 10 dpf zebrafish larvae; Table S1 Oligonucleotide sequences; Table S2 Significantly ($p<0.05$) altered metaboliotes identified in untreated and 0.1 mM pyridoxine-treated 5dpf old *alpl*$^{-/-}$ embryos using one-way ANOVA with Tukey's HSD as the posthoc test; Table S3. Significantly ($p<0.05$) altered metabolites identified with t-test in 10 dpf old *alpl*$^{-/-}$ larvae.

Author Contributions: Conceptualization, J.C., J.J.J and N.M.V.; methodology, J.C., S.M.C.S, N.W.F.M and F.T; validation, J.C., S.M.C.S and M.A.; formal analysis, J.C., S.M.C.S, N.W.F.M, and M.B.; investigation J.C., S.M.C.S, N.W.F.M, and M.B.; resources, J.J.J, N.M.V., J.P.W.B. and G.H.; data curation, J.C.; writing—original draft preparation, J.C.; writing—review and editing, M.A., S.M.C.S, N.W.F.M, F.T., J.P.W.B., G.H., J.J.J and N.M.V.; visualization, J.C.; supervision, G.H., J.J.J and N.M.V.; project administration, J.C.; funding acquisition, M.A., J.J.J and N.M.V. All authors have read and agreed to the published version of the manuscript.

Funding: This work was supported by a Wilhelmina Children's Hospital Research Fund grant to dr. M. Albersen (OZF 2014-2015).

Institutional Review Board Statement: The animal study protocol was approved by the Animal Welfare Body Utrecht, Utrecht University (protocol code 1444WP2B2, 6 April 2022).

Data Availability Statement: Data are available within this manuscript, figures, supplemental figures and supplemental tables. Raw DI-HRMS data are available upon request.

Conflicts of Interest: The authors declare no conflicts of interest.

References

1. J.C. Rathbun, Hypophosphatasia; a new developmental anomaly, Am J Dis Child (1911) 75 (1948) 822-831. 10.1001/archpedi.1948.02030020840003.
2. M.R. Farman, C. Rehder, T. Malli, C. Rockman-Greenberg, K. Dahir, G.A. Martos-Moreno, A. Linglart, K. Ozono, L. Seefried, G. Del Angel, G. Webersinke, F. Barbazza, L.K. John, S.M.A. Delana Mudiyanselage, F. Hogler, E.B. Nading, E. Huggins, E.T. Rush, A. El-Gazzar, P.S. Kishnani, W. Hogler, The Global ALPL gene variant classification project: Dedicated to deciphering variants, Bone 178 (2024) 116947. 10.1016/j.bone.2023.116947.
3. L. Zurutuza, F. Muller, J.F. Gibrat, A. Taillandier, B. Simon-Bouy, J.L. Serre, E. Mornet, Correlations of genotype and phenotype in hypophosphatasia, Hum Mol Genet 8 (1999) 1039-1046. 10.1093/hmg/8.6.1039.
4. I. Brun-Heath, M. Ermonval, E. Chabrol, J. Xiao, M. Palkovits, R. Lyck, F. Miller, P.O. Couraud, E. Mornet, C. Fonta, Differential expression of the bone and the liver tissue non-specific alkaline phosphatase isoforms in brain tissues, Cell Tissue Res 343 (2011) 521-536. 10.1007/s00441-010-1111-4.
5. J.L. Millan, M.P. Whyte, Alkaline Phosphatase and Hypophosphatasia, Calcif Tissue Int 98 (2016) 398-416. 10.1007/s00223-015-0079-1.

 doi:10.20944/preprints202503.0480.v1

6. R.G. Russell, Excretion of Inorganic Pyrophosphate in Hypophosphatasia, Lancet 2 (1965) 461-464. 10.1016/s0140-6736(65)91422-4.
7. R.G. Russell, S. Bisaz, A. Donath, D.B. Morgan, H. Fleisch, Inorganic pyrophosphate in plasma in normal persons and in patients with hypophosphatasia, osteogenesis imperfecta, and other disorders of bone, J Clin Invest 50 (1971) 961-969. 10.1172/JCI106589.
8. K.N. Fedde, M.P. Whyte, Alkaline phosphatase (tissue-nonspecific isoenzyme) is a phosphoethanolamine and pyridoxal-5'-phosphate ectophosphatase: normal and hypophosphatasia fibroblast study, Am J Hum Genet 47 (1990) 767-775.
9. M.P. Whyte, J.D. Mahuren, L.A. Vrabel, S.P. Coburn, Markedly increased circulating pyridoxal-5'-phosphate levels in hypophosphatasia. Alkaline phosphatase acts in vitamin B6 metabolism, J Clin Invest 76 (1985) 752-756. 10.1172/JCI112031.
10. M.P. Whyte, J.D. Mahuren, K.N. Fedde, F.S. Cole, E.R. McCabe, S.P. Coburn, Perinatal hypophosphatasia: tissue levels of vitamin B6 are unremarkable despite markedly increased circulating concentrations of pyridoxal-5'-phosphate. Evidence for an ectoenzyme role for tissue-nonspecific alkaline phosphatase, J Clin Invest 81 (1988) 1234-1239. 10.1172/JCI113440.
11. R.A. McCance, A.B. Morrison, C.E. Dent, The excretion of phosphoethanolamine and hypophosphatasia, Lancet 268 (1955) 131. 10.1016/s0140-6736(55)91704-9.
12. D. Fraser, E.R. Yendt, F.H. Christie, Metabolic abnormalities in hypophosphatasia, Lancet 268 (1955) 286. 10.1016/s0140-6736(55)90112-4.
13. H. Orimo, H.J. Girschick, M. Goseki-Sone, M. Ito, K. Oda, T. Shimada, Mutational analysis and functional correlation with phenotype in German patients with childhood-type hypophosphatasia, J Bone Miner Res 16 (2001) 2313-2319. 10.1359/jbmr.2001.16.12.2313.
14. M.E. Nunes, Hypophosphatasia, in: M.P. Adam, J. Feldman, G.M. Mirzaa, R.A. Pagon, S.E. Wallace, A. Amemiya (Eds.) GeneReviews((R)), Seattle (WA), 1993.
15. J.L. Meyer, Can biological calcification occur in the presence of pyrophosphate?, Arch Biochem Biophys 231 (1984) 1-8. 10.1016/0003-9861(84)90356-4.
16. H. Collmann, E. Mornet, S. Gattenlohner, C. Beck, H. Girschick, Neurosurgical aspects of childhood hypophosphatasia, Childs Nerv Syst 25 (2009) 217-223. 10.1007/s00381-008-0708-3.
17. J. Bacchetta, Renal impairment in hypophosphatasia, Arch Pediatr 24 (2017) 5S93-95S95. 10.1016/S0929-693X(18)30023-X.
18. S. Baumgartner-Sigl, E. Haberlandt, S. Mumm, S. Scholl-Burgi, C. Sergi, L. Ryan, K.L. Ericson, M.P. Whyte, W. Hogler, Pyridoxine-responsive seizures as the first symptom of infantile hypophosphatasia caused by two novel missense mutations (c.677T>C, p.M226T; c.1112C>T, p.T371I) of the tissue-nonspecific alkaline phosphatase gene, Bone 40 (2007) 1655-1661. 10.1016/j.bone.2007.01.020.
19. G.J. Basura, S.P. Hagland, A.M. Wiltse, S.M. Gospe, Jr., Clinical features and the management of pyridoxine-dependent and pyridoxine-responsive seizures: review of 63 North American cases submitted to a patient registry, Eur J Pediatr 168 (2009) 697-704. 10.1007/s00431-008-0823-x.
20. T. Taketani, Neurological Symptoms of Hypophosphatasia, Subcell Biochem 76 (2015) 309-322. 10.1007/978-94-017-7197-9_14.
21. H. Demirbilek, Y. Alanay, A. Alikasifoglu, M. Topcu, E. Mornet, N. Gonc, A. Ozon, N. Kandemir, Hypophosphatasia presenting with pyridoxine-responsive seizures, hypercalcemia, and pseudotumor cerebri: case report, J Clin Res Pediatr Endocrinol 4 (2012) 34-38. 10.4274/jcrpe.473.
22. E. Lefever, P. Witters, E. Gielen, A. Vanclooster, W. Meersseman, E. Morava, D. Cassiman, M.R. Laurent, Hypophosphatasia in Adults: Clinical Spectrum and Its Association With Genetics and Metabolic Substrates, J Clin Densitom 23 (2020) 340-348. 10.1016/j.jocd.2018.12.006.
23. M.L. di Salvo, R. Contestabile, M.K. Safo, Vitamin B(6) salvage enzymes: mechanism, structure and regulation, Biochim Biophys Acta 1814 (2011) 1597-1608. 10.1016/j.bbapap.2010.12.006.
24. M.P. Whyte, F. Zhang, K.E. Mack, D. Wenkert, G.S. Gottesman, K.L. Ericson, J.T. Cole, S.P. Coburn, Pyridoxine challenge reflects pediatric hypophosphatasia severity and thereby examines tissue-nonspecific alkaline phosphatase's role in vitamin B(6) metabolism, Bone 181 (2024) 117033. 10.1016/j.bone.2024.117033.

 doi:10.20944/preprints202503.0480.v1

25. J.M. Colazo, J.R. Hu, K.M. Dahir, J.H. Simmons, Correction to: Neurological Symptoms in Hypophosphatasia, Osteoporos Int 30 (2019) 535. 10.1007/s00198-018-4714-3.
26. M.P. Whyte, C.R. Greenberg, N.J. Salman, M.B. Bober, W.H. McAlister, D. Wenkert, B.J. Van Sickle, J.H. Simmons, T.S. Edgar, M.L. Bauer, M.A. Hamdan, N. Bishop, R.E. Lutz, M. McGinn, S. Craig, J.N. Moore, J.W. Taylor, R.H. Cleveland, W.R. Cranley, R. Lim, T.D. Thacher, J.E. Mayhew, M. Downs, J.L. Millan, A.M. Skrinar, P. Crine, H. Landy, Enzyme-replacement therapy in life-threatening hypophosphatasia, N Engl J Med 366 (2012) 904-913. 10.1056/NEJMoa1106173.
27. G.J. Lieschke, P.D. Currie, Animal models of human disease: zebrafish swim into view, Nat Rev Genet 8 (2007) 353-367. 10.1038/nrg2091.
28. M. Abe, M. Matsuda, A correlation between changes in gamma-aminobutyric acid metabolism and seizures induced by antivitamin B6, J Biochem 80 (1976) 1165-1171. 10.1093/oxfordjournals.jbchem.a131372.
29. D. Liedtke, C. Hofmann, F. Jakob, E. Klopocki, S. Graser, Tissue-Nonspecific Alkaline Phosphatase-A Gatekeeper of Physiological Conditions in Health and a Modulator of Biological Environments in Disease, Biomolecules 10 (2020). 10.3390/biom10121648.
30. H. Van Belle, Alkaline phosphatase. I. Kinetics and inhibition by levamisole of purified isoenzymes from humans, Clin Chem 22 (1976) 972-976.
31. A. Bensimon-Brito, J. Cardeira, M.L. Cancela, A. Huysseune, P.E. Witten, Distinct patterns of notochord mineralization in zebrafish coincide with the localization of Osteocalcin isoform 1 during early vertebral centra formation, BMC Dev Biol 12 (2012) 28. 10.1186/1471-213X-12-28.
32. S.C. Baraban, M.R. Taylor, P.A. Castro, H. Baier, Pentylenetetrazole induced changes in zebrafish behavior, neural activity and c-fos expression, Neuroscience 131 (2005) 759-768. 10.1016/j.neuroscience.2004.11.031.
33. I.A. Pena, Y. Roussel, K. Daniel, K. Mongeon, D. Johnstone, H. Weinschutz Mendes, M. Bosma, V. Saxena, N. Lepage, P. Chakraborty, D.A. Dyment, C.D.M. van Karnebeek, N. Verhoeven-Duif, T.V. Bui, K.M. Boycott, M. Ekker, A. MacKenzie, Pyridoxine-Dependent Epilepsy in Zebrafish Caused by Aldh7a1 Deficiency, Genetics 207 (2017) 1501-1518. 10.1534/genetics.117.300137.
34. J. Ciapaite, M. Albersen, S.M.C. Savelberg, M. Bosma, F. Tessadori, J. Gerrits, N. Lansu, S. Zwakenberg, J.P.W. Bakkers, F.J.T. Zwartkruis, G. van Haaften, J.J. Jans, N.M. Verhoeven-Duif, Pyridox(am)ine 5'-phosphate oxidase (PNPO) deficiency in zebrafish results in fatal seizures and metabolic aberrations, Biochim Biophys Acta Mol Basis Dis 1866 (2020) 165607. 10.1016/j.bbadis.2019.165607.
35. T. Afrikanova, A.S. Serruys, O.E. Buenafe, R. Clinckers, I. Smolders, P.A. de Witte, A.D. Crawford, C.V. Esguerra, Validation of the zebrafish pentylenetetrazol seizure model: locomotor versus electrographic responses to antiepileptic drugs, PLoS One 8 (2013) e54166. 10.1371/journal.pone.0054166.
36. H.A. Haijes, M. Willemsen, M. Van der Ham, J. Gerrits, M.L. Pras-Raves, H. Prinsen, P.M. Van Hasselt, M.G.M. De Sain-van der Velden, N.M. Verhoeven-Duif, J.J.M. Jans, Direct Infusion Based Metabolomics Identifies Metabolic Disease in Patients' Dried Blood Spots and Plasma, Metabolites 9 (2019). 10.3390/metabo9010012.
37. J.E. Baggott, T. Tamura, Metabolism of 10-formyldihydrofolate in humans, Biomed Pharmacother 55 (2001) 454-457. 10.1016/s0753-3322(01)00093-2.
38. L. Brun, L.H. Ngu, W.T. Keng, G.S. Ch'ng, Y.S. Choy, W.L. Hwu, W.T. Lee, M.A. Willemsen, M.M. Verbeek, T. Wassenberg, L. Regal, S. Orcesi, D. Tonduti, P. Accorsi, H. Testard, J.E. Abdenur, S. Tay, G.F. Allen, S. Heales, I. Kern, M. Kato, A. Burlina, C. Manegold, G.F. Hoffmann, N. Blau, Clinical and biochemical features of aromatic L-amino acid decarboxylase deficiency, Neurology 75 (2010) 64-71. 10.1212/WNL.0b013e3181e620ae.
39. L. Nawrocki, R. BreMiller, G. Streisinger, M. Kaplan, Larval and adult visual pigments of the zebrafish, Brachydanio rerio, Vision Res 25 (1985) 1569-1576. 10.1016/0042-6989(85)90127-0.
40. Y. Yang, A.M. Wandler, J.H. Postlethwait, K. Guillemin, Dynamic Evolution of the LPS-Detoxifying Enzyme Intestinal Alkaline Phosphatase in Zebrafish and Other Vertebrates, Front Immunol 3 (2012) 314. 10.3389/fimmu.2012.00314.
41. B. Ohlebusch, A. Borst, T. Frankenbach, E. Klopocki, F. Jakob, D. Liedtke, S. Graser, Investigation of alpl expression and Tnap-activity in zebrafish implies conserved functions during skeletal and neuronal development, Sci Rep 10 (2020) 13321. 10.1038/s41598-020-70152-5.

 doi:10.20944/preprints202503.0480.v1

42. J.L. Millan, S. Narisawa, I. Lemire, T.P. Loisel, G. Boileau, P. Leonard, S. Gramatikova, R. Terkeltaub, N.P. Camacho, M.D. McKee, P. Crine, M.P. Whyte, Enzyme replacement therapy for murine hypophosphatasia, J Bone Miner Res 23 (2008) 777-787. 10.1359/jbmr.071213.
43. K.G. Waymire, J.D. Mahuren, J.M. Jaje, T.R. Guilarte, S.P. Coburn, G.R. MacGregor, Mice lacking tissue non-specific alkaline phosphatase die from seizures due to defective metabolism of vitamin B-6, Nat Genet 11 (1995) 45-51. 10.1038/ng0995-45.
44. K.N. Fedde, L. Blair, J. Silverstein, S.P. Coburn, L.M. Ryan, R.S. Weinstein, K. Waymire, S. Narisawa, J.L. Millan, G.R. MacGregor, M.P. Whyte, Alkaline phosphatase knock-out mice recapitulate the metabolic and skeletal defects of infantile hypophosphatasia, J Bone Miner Res 14 (1999) 2015-2026. 10.1359/jbmr.1999.14.12.2015.
45. S. Narisawa, N. Frohlander, J.L. Millan, Inactivation of two mouse alkaline phosphatase genes and establishment of a model of infantile hypophosphatasia, Dev Dyn 208 (1997) 432-446. 10.1002/(SICI)1097-0177(199703)208:3<432::AID-AJA13>3.0.CO;2-1.
46. D. Belachew, T. Kazmerski, I. Libman, A.C. Goldstein, S.T. Stevens, S. Deward, J. Vockley, M.A. Sperling, A.L. Balest, Infantile hypophosphatasia secondary to a novel compound heterozygous mutation presenting with pyridoxine-responsive seizures, JIMD Rep 11 (2013) 17-24. 10.1007/8904_2013_217.
47. S. Balasubramaniam, F. Bowling, K. Carpenter, J. Earl, J. Chaitow, J. Pitt, E. Mornet, D. Sillence, C. Ellaway, Perinatal hypophosphatasia presenting as neonatal epileptic encephalopathy with abnormal neurotransmitter metabolism secondary to reduced co-factor pyridoxal-5'-phosphate availability, J Inherit Metab Dis 33 Suppl 3 (2010) S25-33. 10.1007/s10545-009-9012-y.
48. S. Narisawa, C. Wennberg, J.L. Millan, Abnormal vitamin B6 metabolism in alkaline phosphatase knock-out mice causes multiple abnormalities, but not the impaired bone mineralization, J Pathol 193 (2001) 125-133. 10.1002/1096-9896(2000)9999:9999<::AID-PATH722>3.0.CO;2-Y.
49. T. Cruz, M. Gleizes, S. Balayssac, E. Mornet, G. Marsal, J.L. Millan, M. Malet-Martino, L.G. Nowak, V. Gilard, C. Fonta, Identification of altered brain metabolites associated with TNAP activity in a mouse model of hypophosphatasia using untargeted NMR-based metabolomics analysis, J Neurochem 140 (2017) 919-940. 10.1111/jnc.13950.
50. S.E. Street, N.J. Kramer, P.L. Walsh, B. Taylor-Blake, M.C. Yadav, I.F. King, P. Vihko, R.M. Wightman, J.L. Millan, M.J. Zylka, Tissue-nonspecific alkaline phosphatase acts redundantly with PAP and NT5E to generate adenosine in the dorsal spinal cord, J Neurosci 33 (2013) 11314-11322. 10.1523/JNEUROSCI.0133-13.2013.
51. O. Kantor, A. Varga, T. Kovacs-Oller, A. Enzsoly, L. Balogh, G. Baksa, Z. Szepessy, C. Fonta, A.W. Roe, R. Nitschke, A. Szel, L. Negyessy, B. Volgyi, A. Lukats, TNAP activity is localized at critical sites of retinal neurotransmission across various vertebrate species, Cell Tissue Res 358 (2014) 85-98. 10.1007/s00441-014-1944-3.
52. K. Laue, H.M. Pogoda, P.B. Daniel, A. van Haeringen, Y. Alanay, S. von Ameln, M. Rachwalski, T. Morgan, M.J. Gray, M.H. Breuning, G.M. Sawyer, A.J. Sutherland-Smith, P.G. Nikkels, C. Kubisch, W. Bloch, B. Wollnik, M. Hammerschmidt, S.P. Robertson, Craniosynostosis and multiple skeletal anomalies in humans and zebrafish result from a defect in the localized degradation of retinoic acid, Am J Hum Genet 89 (2011) 595-606. 10.1016/j.ajhg.2011.09.015.
53. M. Zhong, R. Kawaguchi, B. Costabile, Y. Tang, J. Hu, G. Cheng, M. Kassai, B. Ribalet, F. Mancia, D. Bok, H. Sun, Regulatory mechanism for the transmembrane receptor that mediates bidirectional vitamin A transport, Proc Natl Acad Sci U S A 117 (2020) 9857-9864. 10.1073/pnas.1918540117.
54. S.W. Cho, S. Kim, Y. Kim, J. Kweon, H.S. Kim, S. Bae, J.S. Kim, Analysis of off-target effects of CRISPR/Cas-derived RNA-guided endonucleases and nickases, Genome Res 24 (2014) 132-141. 10.1101/gr.162339.113.
55. I. Brocal, R.J. White, C.M. Dooley, S.N. Carruthers, R. Clark, A. Hall, E.M. Busch-Nentwich, D.L. Stemple, R.N. Kettleborough, Efficient identification of CRISPR/Cas9-induced insertions/deletions by direct germline screening in zebrafish, BMC Genomics 17 (2016) 259. 10.1186/s12864-016-2563-z.
56. J.A. Gagnon, E. Valen, S.B. Thyme, P. Huang, L. Akhmetova, A. Pauli, T.G. Montague, S. Zimmerman, C. Richter, A.F. Schier, Efficient mutagenesis by Cas9 protein-mediated oligonucleotide insertion and large-scale assessment of single-guide RNAs, PLoS One 9 (2014) e98186. 10.1371/journal.pone.0098186.

 doi:10.20944/preprints202503.0480.v1

57. F. Tessadori, H.I. Roessler, S.M.C. Savelberg, S. Chocron, S.M. Kamel, K.J. Duran, M.M. van Haelst, G. van Haaften, J. Bakkers, Effective CRISPR/Cas9-based nucleotide editing in zebrafish to model human genetic cardiovascular disorders, Dis Model Mech 11 (2018). 10.1242/dmm.035469.
58. M.B. Walker, C.B. Kimmel, A two-color acid-free cartilage and bone stain for zebrafish larvae, Biotech Histochem 82 (2007) 23-28. 10.1080/10520290701333558.
59. S. Graser, B. Mentrup, D. Schneider, L. Klein-Hitpass, F. Jakob, C. Hofmann, Overexpression of tissue-nonspecific alkaline phosphatase increases the expression of neurogenic differentiation markers in the human SH-SY5Y neuroblastoma cell line, Bone 79 (2015) 150-161. 10.1016/j.bone.2015.05.033.
60. M. van der Ham, M. Albersen, T.J. de Koning, G. Visser, A. Middendorp, M. Bosma, N.M. Verhoeven-Duif, M.G. de Sain-van der Velden, Quantification of vitamin B6 vitamers in human cerebrospinal fluid by ultra performance liquid chromatography-tandem mass spectrometry, Anal Chim Acta 712 (2012) 108-114. 10.1016/j.aca.2011.11.018.
61. Z. Pang, Y. Lu, G. Zhou, F. Hui, L. Xu, C. Viau, A.F. Spigelman, P.E. MacDonald, D.S. Wishart, S. Li, J. Xia, MetaboAnalyst 6.0: towards a unified platform for metabolomics data processing, analysis and interpretation, Nucleic Acids Res 52 (2024) W398-W406. 10.1093/nar/gkae253.
62. H. Prinsen, B.G.M. Schiebergen-Bronkhorst, M.W. Roeleveld, J.J.M. Jans, M.G.M. de Sain-van der Velden, G. Visser, P.M. van Hasselt, N.M. Verhoeven-Duif, Rapid quantification of underivatized amino acids in plasma by hydrophilic interaction liquid chromatography (HILIC) coupled with tandem mass-spectrometry, J Inherit Metab Dis 39 (2016) 651-660. 10.1007/s10545-016-9935-z.